Spray Coating Experiments: Setups and Methodologies
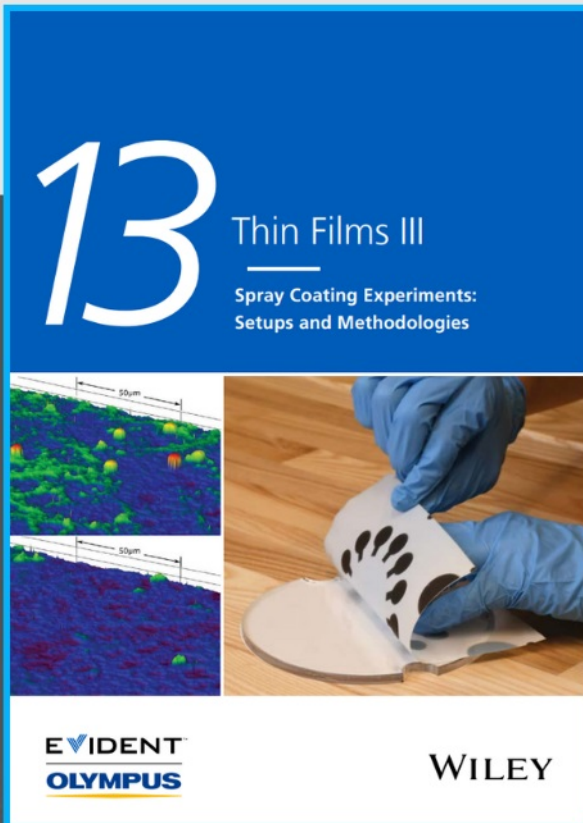
13 Thin Films III

Spray Coating Experiments: Setups and Methodologies

EVIDENT OLYMPUS

WILEY

The latest eBook from Advanced Optical Metrology. Download for free.

Spray Coating Experiments: Setups and Methodologies, is the third in our Thin Films eBook series. This publication provides an introduction to spray coating, three article digests from Wiley Online Library and the latest news about Evident's Image of the Year Award 2022.

Wiley in collaboration with Evident, are committed to bridging the gap between fundamental research and industrial applications in the field of optical metrology. We strive to do this by collecting and organizing existing information, making it more accessible and useful for researchers and practitioners alike.

EVIDENT OLYMPUS

WILEY

Simultaneous Formation of Interphases on both Positive and Negative Electrodes in High-Voltage Aqueous Lithium-Ion Batteries

Xu Hou, Travis P. Pollard, Wenguang Zhao, Xin He,* Xiaokang Ju, Jun Wang, Leilei Du, Elie Paillard, Hai Lin, Kang Xu, Oleg Borodin,* Martin Winter, and Jie Li*

The formation of solid-electrolyte interphase (SEI) in "water-in-salt" electrolyte (WiSE) expands the electrochemical stability window of aqueous electrolytes beyond 3.0 V. However, the parasitic hydrogen evolution reaction that drives anode corrosion, cracking, and the subsequent reformation of SEI still occurs, compromising long-term cycling performance of the batteries. To improve cycling stability, an unsaturated monomer acrylamide (AM) is introduced as an electrolyte additive, whose presence in WiSE reduces its viscosity and improves ionic conductivity. Upon charging, AM electropolymerizes into polyacrylamide, as confirmed both experimentally and computationally. The in situ polymer constitutes effective protection layers at both anode and cathode surfaces, and enables $LiMn_2O_4$‖L-TiO_2 full cells with high specific capacity (157 mAh g^{-1} at 1 C), long-term cycling stability (80% capacity retention within 200 cycles at 1 C), and high rate capability (79 mAh g^{-1} at 30 C). The in situ electropolymerization found in this work provides an alternative and highly effective strategy to design protective interphases at the negative and positive electrodes for high-voltage aqueous batteries of lithium-ion or beyond.

1. Introduction

Rechargeable aqueous lithium-ion batteries (ALIBs) have been considered promising battery systems due to their high safety, low cost, and environmental benignancy.[1] However, the narrow electrochemical stability window (ESW) of aqueous electrolytes limits the operating voltage and hence excludes the adoption of high energy electrode materials that often operate at extreme potentials.[2] In particular, H_2 and O_2 evolution reactions (HER and OER) that originate from water decomposition at the fully charged state may severely deteriorate the electrode structure, resulting in fast capacity fading.[3] The concept of highly concentrated aqueous electrolytes, as represented by the so-called "water-in-salt" electrolytes (WiSEs), was introduced by Suo et al.[4] and Yamada et al.[5] and significantly expanded the ESW of aqueous solution from 1.23 V to ≈3.0 V via the formation of interphases. In those electrolytes HER and OER are altogether suppressed, resulting in enhanced cycling stability of ALIBs. However, the solid-electrolyte interphase (SEI) therein is often not stable on the long-term during cycling as cracking, dissolution, and continuous reforming occurs,[6] thus leading to capacity fade.

X. Hou, X. Ju, E. Paillard, M. Winter, J. Li
Helmholtz-Institute Muenster (HI MS)
IEK-12
Forschungszentrum Juelich GmbH
Corrensstr. 46, 48149 Muenster, Germany
E-mail: jie1.li@polimi.it
T. P. Pollard, K. Xu, O. Borodin
Battery Science Branch
Sensor and Electron Devices Directorate
US Army Research Laboratory
Adelphi, MD 20783, USA
E-mail: oleg.a.borodin.civ@mail.mil

W. Zhao, H. Lin
School of Advanced Materials
Shenzhen Graduate School
Peking University
Shenzhen 518055, China
X. He
School of Chemical Engineering
Sichuan University
Chengdu 610065, China
E-mail: xinhe@scu.edu.cn
J. Wang
Academy for Advanced Interdisciplinary Studies
Southern University of Science and Technology
Shenzhen 518055, China
L. Du, M. Winter
MEET Battery Research Center
Institute of Physical Chemistry
University of Muenster
Corrensstr. 46, 48149 Muenster, Germany
E. Paillard, J. Li
Department of Energy
Politecnico di Milano
Via Lambruschini 4, Milano, MI 20156, Italy

To enhance the cycling stability of ALIBs, numerous strategies have been proposed to reinforce the aqueous interphases that include both SEI on the anode and cathode-electrolyte interphase (CEI) on the cathode.[1b,7] 1) Further increase of salt concentration has been pursued, with the salt/water ratio reaching as high as 1.0[8] and 1.13,[9] respectively. However, this approach sees very limited increase in ESW at the expense of high cost and high viscosity.[10] 2) Other approaches focus on interphasial chemistry by introducing film-forming electrolyte additives, such as tris(trimethylsilyl) borate (TMSB) that was used to stabilize $LiCoO_2$ by forming an effective CEI through electrochemical oxidation,[11] or divalent salts (Mg (TFSI)$_2$ and Ca (TFSI)$_2$) that were used to form a less-soluble SEI (MgF_2, $MgCO_3$, CaF_2 or $CaCO_3$, etc.) in WiSE.[12] 3) Organic solvents were also added to provide non-aqueous source to SEI chemistry, as in water/DMC or water/acetonitrile hybrid electrolytes.[13] However, none of these approaches provide sufficient long-term protection of electrodes at extreme potentials.

The SEI additives currently adopted in LIBs often involve in situ electropolymerization of a monomer, such as vinylene carbonate (VC),[14] isocyanate,[15] and acrylonitrile[16] or even fluoroethylene carbonate, which is not a monomer by itself but its dehydrofluorination produces LiF and VC. These polymerizable additives have been proven to be an effective method to form robust SEI and CEI at the electrode|electrolyte interfaces. In addition, Stojkovic et al.[17] reported the use of VC as an additive in an aqueous battery. By adding 1 wt.% VC into a saturated aqueous $LiNO_3$ solution, the initial discharge capacity of a $Li_{1.05}Cr_{0.1}Mn_{1.85}O_4$||$V_2O_5$ cell was enhanced as well as the cycling stability. The crucial function of the VC-derived SEI is, in this case, the suppression of the penetration of free water to the electrode surface.

Herein, we report an approach of using the acrylamide (AM) as electrolyte additive. Its polymeric form, polyacrylamide (PAM), has been well established as an effective corrosion inhibitor for metals by preferential chemical adsorbing on the metal surfaces and suppressing HER thereafter.[18] However, direct use of PAM is not favored, as its aqueous solutions display high viscosity, which is harmful to the electrolyte conductivity and the wettability of the electrolyte with electrodes and separator.[19] The monomeric AM in aqueous solutions, however, does not bring high viscosity, and could be electropolymerized on demand when the electrodes are charged. These combined merits of AM make it a highly promising chemical source for both SEI and CEI in aqueous electrolytes.

2. Results and Discussions

2.1. Structural and Physicochemical Properties

AM was added to WiSE, that is, 21 m lithium bis(trifluoromethane sulfonyl)imide (LiTFSI) in water, and the resulting electrolyte is denoted WiSE-A$_x$ (m$_{AM}$: m$_{H2O}$ = x%) hereafter, whose structures were investigated via FTIR spectroscopy. Compared with the WiSE, five new signals at 988, 1459, 1589, 1688, and 3387 cm^{-1} are observed upon the addition of AM, which are attributed to =C−H bending, −C−H bending, −C=C stretching, −C=O stretching, and −N−H stretching

mode, respectively (**Figure 1**a–c). The peak intensities increase with the increase of AM content. The structure of the Li$^+$ primary solvation sheath is obviously affected by AM, which is seen via the increased intensity of signals for free water (at 1633 and 3250 cm^{-1}), as well as the decreased signals for water in Li$^+$ solvation sheath, that is, at 3555 and 3620 cm^{-1}. Both indicators strongly suggest the replacement of water by AM in the Li$^+$ solvation sheath.
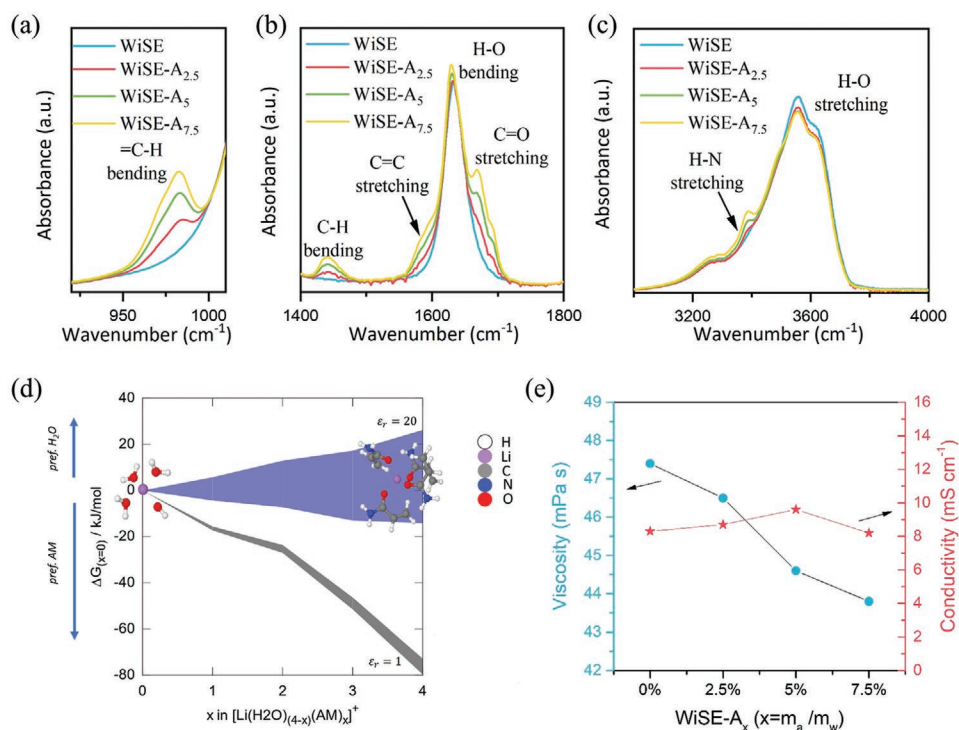
The relative stability of the Li$^+$(H$_2$O)$_{(4-x)}$(AM)$_x$ solvates was evaluated using M052X/6-31+G(d,p) Density functional theory (DFT) calculations as shown in Figure 1d in the gas phase and with the solvates immersed in a polarized continuum solvent model with ε = 20. The solvate free energy was calculated relative to Li$^+$(H$_2$O)$_4$, with bulk-water represented as the cage and prism configurations of the water hexamer and bulk-AM through the dimer and tetramer structures. Substitution of water for AM is clearly favored in gas-phase. Submersion of the Li$^+$(H$_2$O)$_{(4-x)}$(AM)$_x$ solvates in the continuum solvent with ε = 20 shows that all solvates have similar relative free energy, with the DFT results depending somewhat on the bulk-like reference state of AM (the tetramer state gives the stronger preference for replacing water). Thus, in accord with the FTIR observations, DFT calculations show that AM partially replaces water in the Li$^+$ first solvation sheath with the replacement being more pronounced near the electrode surfaces, where electrolyte dielectric constant is expected to decrease.

The viscosity and ionic conductivity of WiSE-A$_x$ electrolytes are compared in Figure 1e and Table S1, Supporting Information. The viscosity decreases gradually with the addition of AM, resulting in good electrolyte wettability in practical battery assembly and operation. Due to decreasing electrolyte viscosity with AM presence, the ionic conductivity of WiSE-A$_x$ electrolytes initially increases slightly and then decreases when the content of AM becomes higher than 5%, as the higher fraction of the Li$^+$ become solvated by the bulkier AM versus water would likely lead to lower mobility of the solvated Li$^+$ or increasing salt aggregation. The thermal behavior of WiSE-A$_x$ electrolytes was investigated by DSC measurements as shown in Figure S1, Supporting Information. Both peritectic temperature (T_p) and liquidus temperature (T_L) of WiSE-A$_x$ decrease with the increase of AM content, demonstrating that the addition of AM in WiSE-A$_x$ allows extending the liquid range toward at low temperatures.

2.2. Electrochemical Stability Window (ESW)

The ESW of WiSE-A$_x$ electrolytes was evaluated by CV measurements, as shown in **Figure 2**a and in the magnified view of the regions near cathodic and anodic potential extremes in Figure 2b,c. WiSE-A$_5$ shows the lowest reduction potential limit, which is crucial for the utilization of active negative electrode materials with low redox potential, such as TiO_2. The cathodic current in the range from 2.8 to 1.9 V (versus Li|Li$^+$), which is related to the HER and reduction of TFSI$^-$ anion, decreases first with AM-content (in WiSE-A$_{2.5}$ and WiSE-A$_5$) and then increases to values even higher than in WiSE, when the additive amount is over 7.5%. This phenomenon is attributed to the change in the Li$^+$ solvation sheath due to the addition of AM in

**ADVANCED
SCIENCE NEWS**

www.advancedsciencenews.com

NANO · MICRO

small

www.small-journal.com

Figure 1. ATR-FTIR absorbance spectra of a series of WiSE-A_x electrolytes (x = 0, 2.5, 5, 7.5) with wavenumber ranging from a) 920 to 1010 cm^{-1} and b) 1400 to 1800 cm^{-1}, c) 3000 to 4000 cm^{-1}. d) Relative binding free energies of Li(H$_2$O)$_{(4-x)}$(AM)$_x$ clusters in gas phase (grey curve) and in polarized continuum solvent (in blue, with ε = 20 to mimic lower dielectric of WiSE compared to water is used). The spread reflects the largest energy differences between (H$_2$O)$_6$ cage and prism configurations and AM dimer and tetramer configurations used as the reference states to compute binding energies. e) The viscosity and conductivity of WiSE-A_x electrolytes at 30 °C.

the electrolyte as illustrated in Figure S2, Supporting Information. Since the Li$^+$ solvation sheath adsorbs at the electrode surface before hydrogen evolution and reduction of TFSI$^-$ occur,[20] the structural changes induced in the Li$^+$ solvation sheaths by AM result in less adsorbed water on the electrode surface, leading to suppressed HER and reduced current density. However, the dielectric constant of electrolyte decreases with the addition of AM, resulting in fast reduction of water when the additive amount is over 7.5%.

At high potential, both AM and TFSI$^-$ anions adsorb on the electrode surface, which can protect the electrolyte from OER.[21] However, because the oxidation of AM occurs at 4.4 V (versus Li|Li$^+$),[22] the oxidation potential of WiSE-A_x decreases with the addition of AM. Overall, the difference between WiSE-$A_{2.5}$ and WiSE-A_5 is negligible within the considered voltage window, which only becomes pronounced below 1.9 V (versus Li|Li$^+$). Given the higher ionic conductivity of WiSE-A_5 compared with WiSE-$A_{2.5}$, WiSE-A_5 was selected for further electrochemical characterizations, specifically for LiMn$_2$O$_4$‖TiO$_2$ full cell tests.

2.3. In Situ Electropolymerization

As shown in Figure S3, Supporting Information, there is a crossover or "nucleation loop" in the low potential range of CV curve in the electrolyte with AM additive during the first cycle. This phenomenon is attributed to the nucleation

process of polymer film formation on the electrode surface, which is caused by electrodeposition or electropolymerization.[23] It is anticipated that electropolymerization of AM is initiated reductively when scanning to low potential. From the SEM image of the working electrode recovered from CV measurement in WiSE-A_5 electrolyte (Figure 2d), an apparent membrane covering the surface can be observed, which can be ascribed to the electropolymerized PAM. Comparing the four electrolytes after 20 cycles in CV measurements (Figure 2e), it shows that the viscosities increase proportionally to the concentration of AM, due to the formation of PAM, which results in a high viscosity after in situ electropolymerization. To further confirm, ATR-FTIR of the WiSE-A_5 electrolyte was conducted following the CV measurement. The intensities of the characteristic peaks of =C—H bending and C=C stretching at 980 and 1585 cm^{-1} become obviously lower when compared with the pristine WiSE-A_5 and WiSE-P_5 electrolyte (Figure 2f,g). Hence, the concentration of AM decreases as a result of its electropolymerization.

DFT calculations were used to investigate the possibility of in situ electropolymerization reaction. Three mechanisms were considered as sources for initiating the polymerization of the AM monomer: 1) anion reduction, 2) partial HER, and 3) direct reduction of the AM species. Figure S4a, Supporting Information, shows the highest reduction potential observed for direct reduction of free (not Li$^+$ bound) AM dimers, highlighting a preference for leveraging the radical H· generated through the partial HER process. H· adds to the alkene, generating
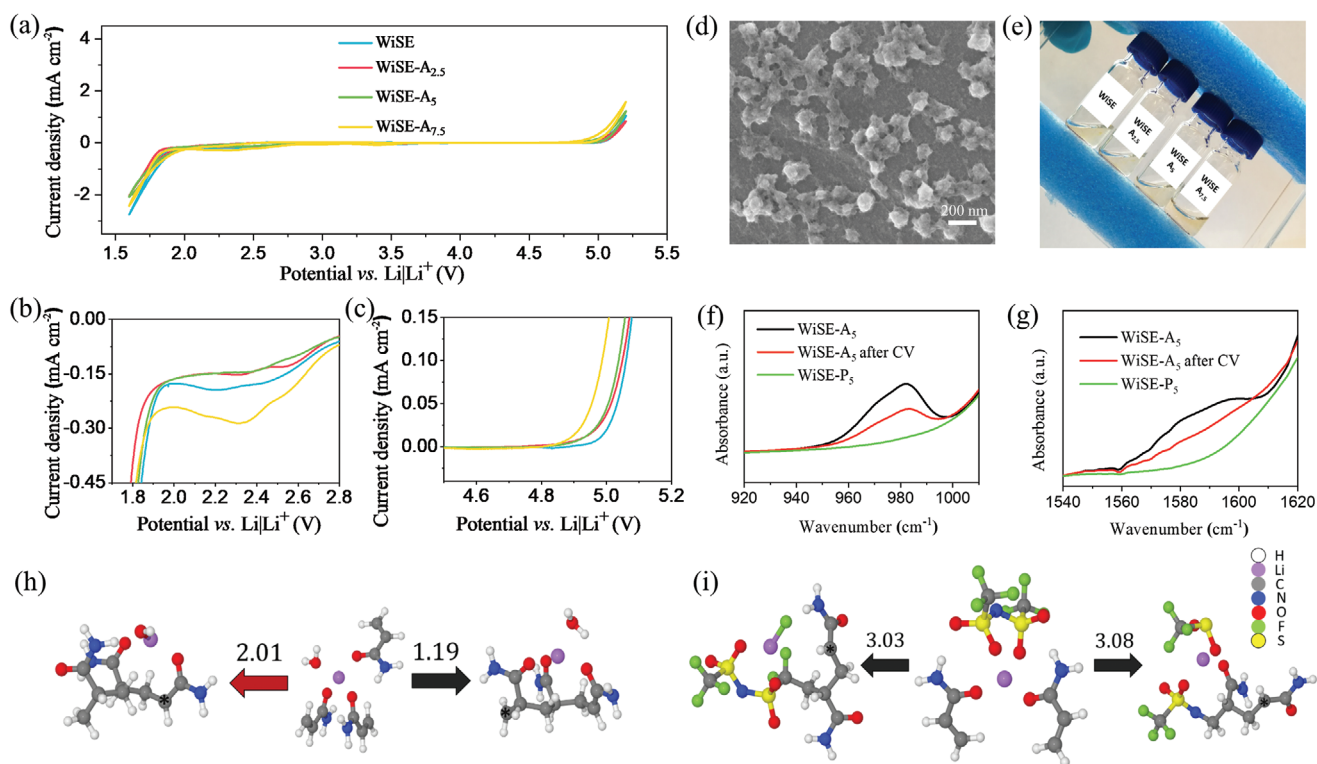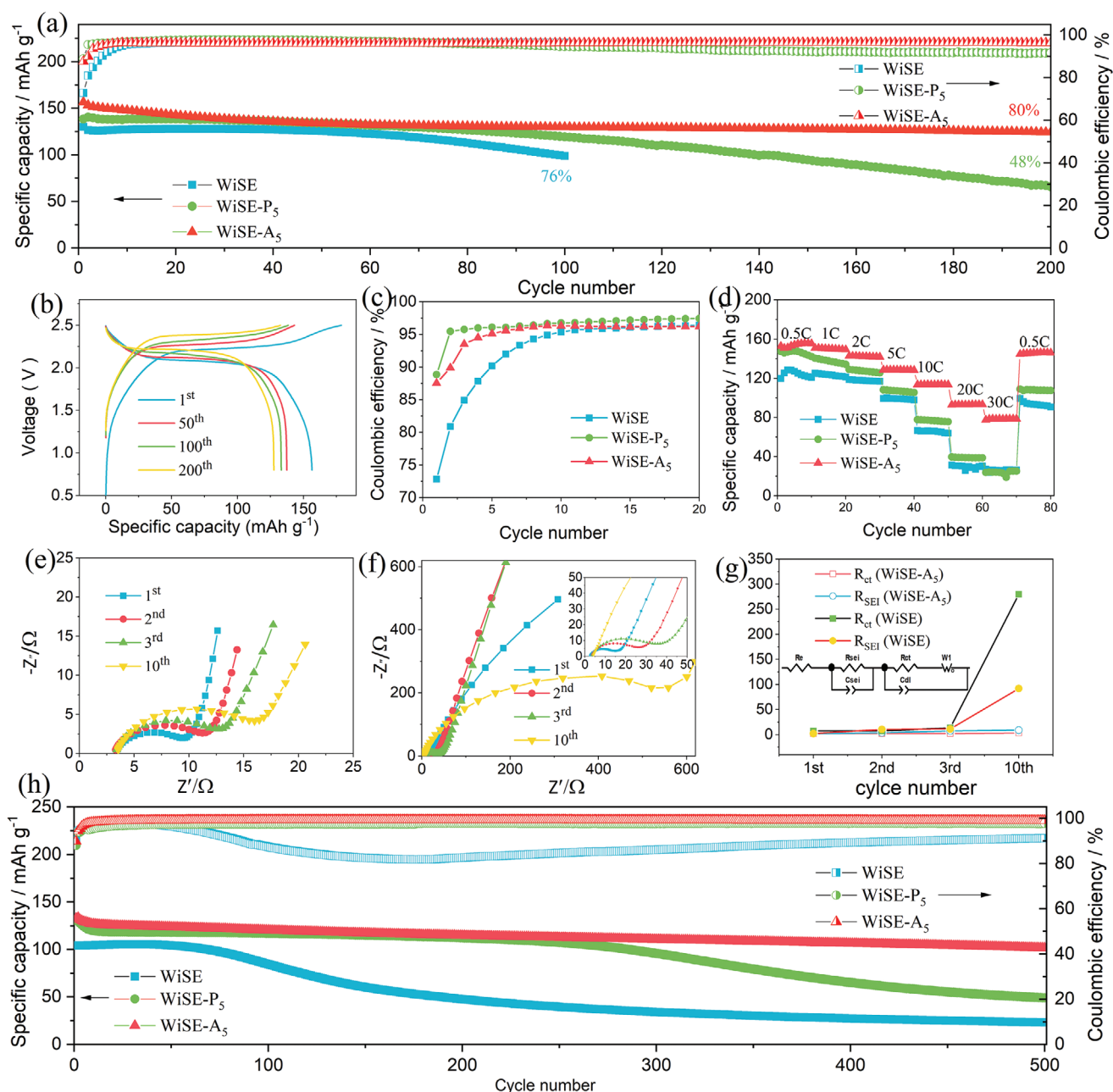
Figure 2. a) CV measurements for the ESW of a series of WiSE-A$_x$ electrolytes (x = 0, 2.5, 5, 7.5) between 1.6 and 5.2 V (versus Li|Li$^+$) at 10 mV s^{-1}. Stainless steel is used as working electrode. b,c) Magnified view of the regions near anodic and cathodic extremes in (a). d) The SEM image of stainless-steel working electrode after CV scanning 20 cycles in WiSE-A$_5$. e) Picture of a series of WiSE-A$_x$ after CV measurements. f,g) ATR-FTIR absorbance spectra of pristine WiSE-A$_5$, pristine WiSE-P$_5$, and WiSE-A$_5$ after CV scanning 20 cycles. h) The reduction potential of Li$^+$(H$_2$O)$_1$(AM)$_3$ species (V versus Li|Li$^+$). A colored arrow points left (red) if the reduction initiates AM polymerization through partial hydrogen evolution and the addition of H · to the AM alkene. A black arrow points to the right to show the product evolved from reduction of one of the AM monomers directly. i) Reduction potentials (versus Li|Li$^+$) showing TFSI$^-$ reduction driven initiation of the AM electropolymerization reaction. The radical fragment derived from anion reduction adds at the alkene carbon.

terminal CH$_3$ and pushing the radical onto the internal CH site. These processes occur below the voltage range of interest, implying that Li$^+$ coordination of AM may direct the preferential electropolymerization of those AM molecules in the solvation sheath. Indeed, it is observed in Figure S4b–e, Supporting Information, that incremental substitution of more AM into the solvation sheath leads to a general increase in the reduction potential (assuming that all Li-coordinated AM monomers polymerize). The reduction potentials for direct reduction of Li-coordinated AM do not reach the voltage window of interest either, though the Li$^+$(H$_2$O)$_2$(AM)$_2$ and Li$^+$(H$_2$O)$_1$(AM)$_3$ species do assume HER as a source of the initiator with voltages in the range of 1.8 to 2 V versus Li|Li$^+$ (Figure 2h). The highest reduction voltages, occurring around 3 V versus Li|Li$^+$, were observed for the water-free LiTFSI(AM)$_2$ cluster (Figure 2i). The high reduction potential reflects the stabilization of CF$_2$SO$_2$NSO$_2$CF$_3$ or NSO$_2$CF$_3$ radicals induced by the addition at the alkene of the monomers and the subsequent polymerization. Overall, DFT calculations predict that the electropolymerization is initiated by AM combining with primarily radicals coming from TFSI$^-$ reduction > HER > and reduction of AM itself. There is also a preference for coordination with Li$^+$ and greater AM coordination number in the case of self-initiated or HER induced polymerization.

2.4. Electrochemical Performance

With the enhanced electrochemical stability at low potentials provided by the electropolymerization of AM in WiSE, WiSE-A$_5$ can support anode materials with low redox potentials, for example, TiO$_2$. Thus, a LiMn$_2$O$_4$‖TiO$_2$@LiTi$_2$(PO$_4$)$_3$ (LiMn$_2$O$_4$ and the self-synthesized LiTi$_2$(PO$_4$)$_3$ coated TiO$_2$ were noted as LMO and L-TiO$_2$, respectively) full cell with WiSE-A$_5$ was constructed in a 2032-type coin cell configuration. The mass loadings of negative electrode and positive electrode were ≈2 and 4 mg cm^{-2}, respectively. The cells are cycled between 0.8–2.5 V at 1 C (1 C = 150 mA g^{-1}). During the first cycle, the full cell with WiSE-A$_5$ delivers a discharge capacity of 157 mAh g^{-1} (calculated based on L-TiO$_2$ electrode, hereafter) with a Coulombic efficiency (CE) of 88% (**Figure 3**a), showing the highest discharge capacity when compared with WiSE (130 mAh g^{-1}, CE of 73%) and WiSE-P$_5$ (138 mAh g^{-1}, CE of 89%), which is ascribed to the lower resistance and suppression of the HER in WiSE-A$_5$. Such an LMO‖L-TiO$_2$ full cell delivers a voltage plateau at 2.0–2.3 V during the discharging and charging process (Figure 3b), and an energy density of 105 Wh kg^{-1} based on the first discharge curve, higher than those with WiSE (88 Wh kg^{-1}) or WiSE-P$_5$ (90 Wh kg^{-1}) electrolyte. In addition, using WiSE-A$_5$, a high capacity of 124 mAh g^{-1} is maintained

ADVANCED
SCIENCE NEWS
www.advancedsciencenews.com

NANO · MICRO
small
www.small-journal.com

Figure 3. Comparison of electrochemical performance of LMO∥L-TiO$_2$ full cell with WiSE, WiSE-P$_5$ and WiSE-A$_5$ electrolytes between 0.8–2.5 V at 1 C. a) the cycling stability and CE, b) charge/discharge profiles of 1st, 50th, 100th, and 200th cycles with WiSE-A$_5$, c) Magnified view of the CEs at first 20 cycles, d) the rate performance. e,f) Nyquist plots full cells with e) WiSE-A$_5$ and f) WiSE after cycling 1, 2, 3, 10 cycles. g) Fitting results of R_{ct} and R_{SEI} form EIS. h) Long-term cycling performance at 5 C. (Both capacity and rate are based on the mass of L-TiO$_2$).

after 200 cycles (80% capacity retention) with a high CE of 96%. In the absence of AM, the full cell with WiSE only maintains 76% of initial discharge capacity after only 100 cycles. Moreover, although the capacity and cycling stability are enhanced with PAM additive, the capacity fades gradually after 100 cycles and the CE drops correspondingly. Only 48% of the initial capacity can be obtained after 200 cycles with a CE of 91%. Therefore, it is expected that more effective SEI and CEI are formed in the full cell using WiSE-A$_5$. Comparing the CE of the full cell with different electrolytes during the first 20 cycles (Figure 3c), the

longest activation process, which is an indicator of interphase effectiveness and defined as the cycle numbers needed for 95% to stabilize, is observed for WiSE (>10 cycles), while the shortest activation process is for WiSE-P$_5$ where it took only 5-cycle to reach a stable CE.

An LMO∥L-TiO$_2$ full cell with WiSE-A$_5$ also demonstrates enhanced rate capability and long-term cycle stability (Figure 3d). A high capacity of 79 mAh g^{-1}, approximately 52% of its capacity at 0.5 C, can be reached at 30 C, which corresponds to a charge time of 2 min. Moreover, when the current

rate is returned to 0.5 C after high rates cycling up to 30 C, the cell resumes a capacity of 146 mAh g^{-1}, which is comparable to the initial capacity. The significantly improved rate capability demonstrates that although the viscosity increases after in situ electropolymerization, the ionic conductivity of the electrolyte actually increases by adding AM in WiSE. Meanwhile, good wettability of the electrodes is already achieved before cycling since WiSE-A$_5$ shows lower viscosity than WiSE. Therefore, the full cell with WiSE-A$_5$ delivers higher reversible capacity as well. In contrast, full cells with WiSE and WiSE-P$_5$ show low capacity retentions at high rates, with a similar value of ≈26 mAh g^{-1} for both, which is 21% and 18% of their initial capacity at 0.5 C, respectively. To better understand the influence of SEI and CEI on rate capability, EIS measurements were performed on LMO∥L-TiO$_2$ full cells with either WiSE-A$_5$ or WiSE (Figure 3e–g). The former has a far lower cell impedance than the latter because of the lower interfacial resistance, higher ionic conductivity, and better wettability of WiSE with AM additive, resulting in a better rate capability. Furthermore, due to the electrolyte decomposition at the electrode surface with WiSE during cycling, a high R_{sei} of 92.2 Ω is obtained in the cell with WiSE after only 10 cycles, as compared with 9.1 Ω in presence of AM. Therefore, the SEI and CEI formed by AM not only protects the electrolytes from excessive decomposition but also remains thin and ionically conductive. More importantly, the full cell with WiSE-A$_5$ also shows good long-term cycling stability (Figure 3h). After 500 cycles a high capacity of 102 mAh g^{-1} is delivered at 5 C with a slow fading of 0.05% per cycle, much lower than the cells with WiSE and WiSE-P$_5$ cells.

To understand how robust the interphases are, self-discharge experiments were conducted. The evolution of open circuit voltages (OCV) of a fully charged LMO∥L-TiO$_2$ cells with WiSE and WiSE-A$_5$ were compared in Figure S5, Supporting Information, where, after charge and discharge at 1 C for 5 cycles, the OCV is stable in the fully charged state with WiSE-A$_5$ but suffers a drastic drop with WiSE. Previous literature has demonstrated that the SEI evolved from WiSE is inhomogeneous with defects such as cracks and holes because of the competition of HER and incessant dissolution of SEI components during the formation of SEI.[6b] Holes appear in the SEI due to the dissolution of SEI components, that is, LiF and Li$_2$CO$_3$, thus exposing the electrode surface. Cracks developed due to the mechanical impact by H$_2$ gas bubbles from further decomposition of electrolyte. As a result, a thick but loosely structured SEI forms, leading to a high cell resistance and severe OCV decay. Adding AM in WiSE results in a denser and thinner SEI.

2.5. Post Mortem Analysis

The chemical composition of the interphases on both L-TiO$_2$ and LMO electrodes were investigated by X-ray photoelectron spectroscopy (XPS) after cycling in WiSE-A$_5$ over 100 cycles (**Figure 4**). On L-TiO$_2$ electrode, as shown in Figure 4a–c, F 1s signals from PVdF and LiF are detected at 688.1 and 685.8 eV, while C 1s signals can be deconvoluted into contributions from C─C species (284.8 eV), C─H (285.6 eV), O=C─N (287.6 eV), ─CF$_2$ (291.1 eV) and Li$_2$CO$_3$ (289.9 eV). Compared with WiSE,[24] the signal at 287.6 eV observed from the electrode

cycled in WiSE-A$_5$ clearly arises from a species related to the amide group from PAM. Additionally, the signal at 400.4 eV in the N 1s spectrum can also be assigned to O=C─N coming from the PAM polymer. Therefore, it can be deduced that AM participates in SEI formation and contributes interphase species similar to those from PAM. The depth profiles of F 1s, N 1s, and C 1s spectra (Figure S6, Supporting Information, and Figure 4d–f) reveal that the content of LiF increases with the depth, while O=C─N species from PAM and Li$_2$CO$_3$ remain relatively constant, suggesting that the SEI consists of a LiF rich inner layer with uniform distribution of polymer throughout.

The F 1s, N 1s, and C 1s XPS spectra collected on cycled LMO cathode are shown in Figure 4g–i, which clearly demonstrates the contribution of LiF, PAM, and Li$_2$CO$_3$ to the formation of the CEI. Similar to the SEI, ─CF$_3$ and R─S─N─S species coming from TFSI$^-$ are observed from F 1s (689.2 eV), C 1s (293.2 eV), and N 1s (399.6 eV) spectra, indicating the participation of TFSI$^-$ in the CEI layer in addition to AM products. The evolution of PAM and TFSI$^-$ species in the CEI near the OER potential were explored with DFT calculations, as shown in Figure 5. A trimer model capped with methyl groups is used as a stand-in for the polymer. Calculations are performed with and without TFSI$^-$ to stabilize the hole. Oxidation occurs at the backbone CH site and is accompanied by a proton transfer to H$_2$NCOH in the range of 4.05–4.14 V versus Li∣Li$^+$ (blue arrows in **Figure 5**a–c). Acidification of the NH$_2$ or release of NH$_3$ with ring closure occurs at higher potentials in Figure 5a,b (orange and green arrows). The radical can be easily oxidized again to a carbocation, which may participate in cross-linking or possibly chemisorb to the cathode surface preventing metal dissolution (Figure 5c,d). PAM appears to also be more resistant to direct oxidative acidification of TFSI$^-$ as discussed with polyethylene oxide which is not observed until a ≈5.8 V versus Li∣Li$^+$ (Figure 5e).[25] Initiation of the polymerization reaction may arise from products generated via OER, with the hydroxyl radical as the initiator at ≈3.5 V versus Li∣Li$^+$ (Figure 5f). Depth profiling (Figure S7, Supporting Information, and Figure 4j–l) shows relatively uniform distribution of LiF and PAM from outer layer to inner layer. Similar trends can be observed for LiF and Li$_2$CO$_3$ signals when cycled in WiSE (Figure S8, Supporting Information), suggesting that PAM indeed participates in the composition of CEI layer but bring no negative effect on the reaction of CEI formation from LiTFSI. Therefore, a uniform and compact CEI not only prevents the dissolution of metal ions from the active material but also facilitates Li-ion transport through the interface.

SEM and TEM images of L-TiO$_2$ and LMO, collected after cycling in WiSE and WiSE-A$_5$, are displayed in Figure 6. On the one hand, compared with the pristine electrode (Figure S9, Supporting Information), the SEM images of cycled L-TiO$_2$ electrodes (**Figure 6**a,b) show no obvious difference between the two electrolytes. However, HRTEM images shown in Figure 6e,f, reveal that the L-TiO$_2$ electrode cycled in WiSE is covered under a non-uniform surface layer with a 5–10 nm thickness derived from the continuous deposition of reduction products of LiTFSI and the formation of Li$_2$CO$_3$. However, when cycled in WiSE-A$_5$, a ≈3 nm thick surface layer develops on the particle surface of L-TiO$_2$, suggesting that the in situ electropolymerization of AM leads to a denser
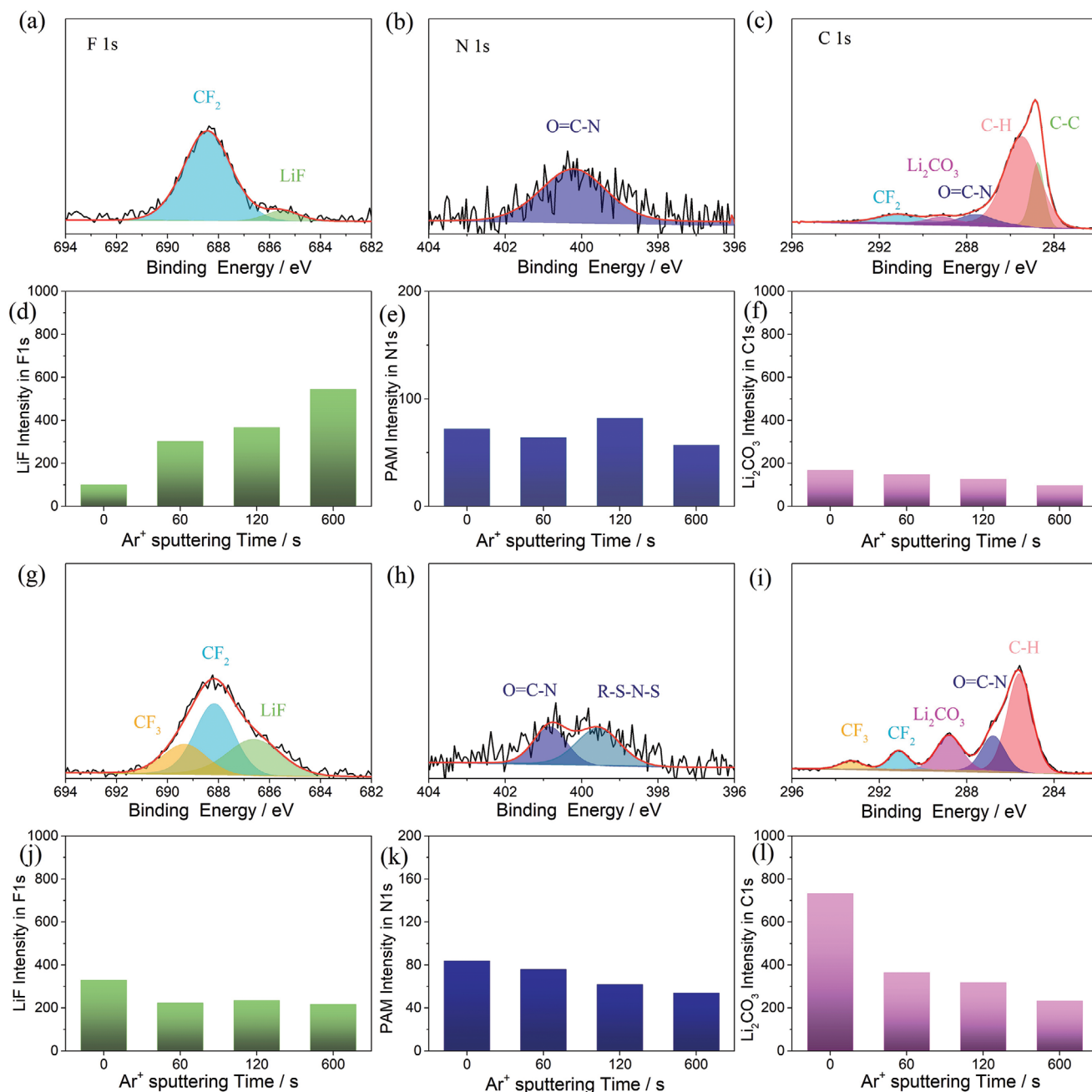
Figure 4. XPS spectra of L-TiO$_2$ electrode and LMO electrode a,g) F 1s, b,h) N 1s, c,i) C 1s after cycling in the full cell with WiSE-A$_5$ for 100 cycles, respectively. d–f) and j–l) The intensity changes of LiF from F 1s, PAM from N 1s, and Li$_2$CO$_3$ from C 1s with various durations of Ar$^+$ sputtering for L-TiO$_2$ electrode and LMO electrode, respectively.

SEI layer. This layer suppresses further reduction of LiTFSI on the anode surface and slows the gradual growth of SEI layer. On the cathode, a discontinuous CEI can be found with WiSE (Figure 6c), comprised of a loose porous layer with a thickness of ≈60 nm according to TEM (Figure 6g). A much smoother surface is observed for the LMO electrode cycled with WiSE-A$_5$ (Figure 6d). HRTEM shows a denser layer with a thickness of ≈15 nm (Figure 6h), suggesting that in situ electropolymerization of AM contributes to form a robust and uniform CEI.

3. Conclusion

A new in situ electropolymerization strategy is introduced to reinforce the SEI and CEI chemistries for high-voltage ALIBs. The addition of AM in WiSE results in a lower viscosity and higher ionic conductivity, which is beneficial for electrode wetting and cell assembly. The replacement of water by AM in the Li$^+$ solvation sheath suppresses hydrogen evolution during the first lithiation of the anode (1.9–2.8 V versus Li|Li$^+$). The in situ electropolymerization of AM to PAM was identified by computation
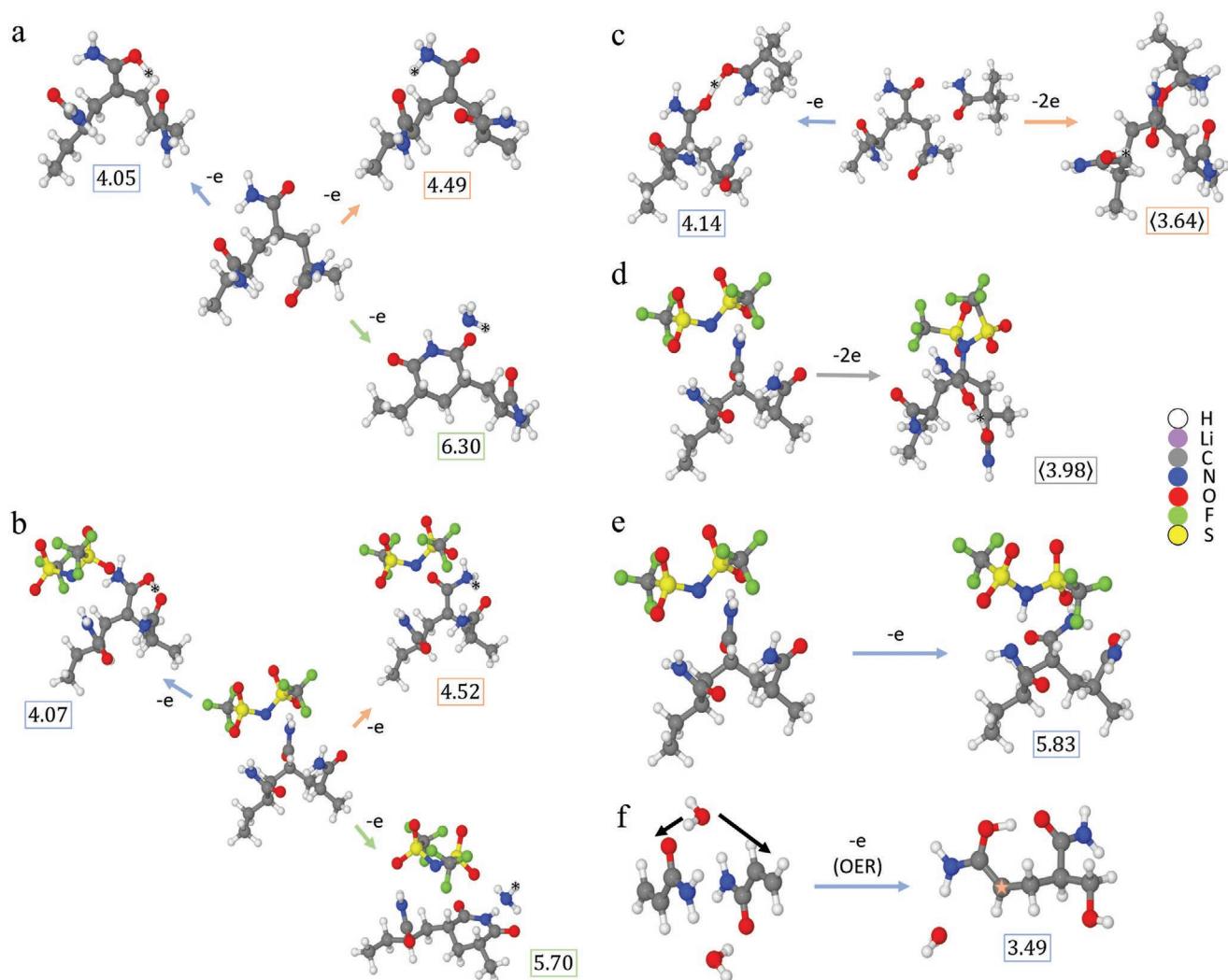
Figure 5. a) Oxidation potential (in V versus Li|Li⁺) of PAM-TFSI coupled with proton transfer at CH site to C=O, NH₂, and ring close after release of NH₃. b) Single-electron oxidation as in (a), but with TFSI⁻ present. c) Single oxidation to acidify second PAM molecule (intermolecular proton transfer) and the average potential from a 2-electron oxidation leading to intramolecular proton transfer and branching/crosslinking to quench the carbocation. d) Average potential from 2-electron oxidation to quench carbocation by binding TFSI⁻. e) Oxidation leading to TFSI⁻ acidification (HTFSI). f) Initiation of polymerization through 1-electron part of the OER, the star denotes the site of the radical for continued polymer growth. OH adds at one of the terminal alkene carbons, H⁺ adds to carbonyl C=O in this case.

and experiment to be responsible for the new interphase on both the anode and cathode. The benefits of an AM-derived SEI and CEI in WiSE over baseline WiSE are demonstrated through excellent performance of an LMO‖L-TiO₂ full cell, achieving: 1) higher reversible capacity (157 mAh g⁻¹), 2) better cycling stability (80% capacity retention after 200 cycles at 1 C) as well as better rate capability (79 mAh g⁻¹ at 30 C), and 3) long-term cycling stability (102 mAh g⁻¹ after 500 cycles at 5 C). These results highlight in situ electropolymerization as a viable strategy to enhance the cycle and calendar life of high-voltage aqueous batteries based on both lithium-ion and beyond.

Supporting Information

Supporting Information is available from the Wiley Online Library or from the author.
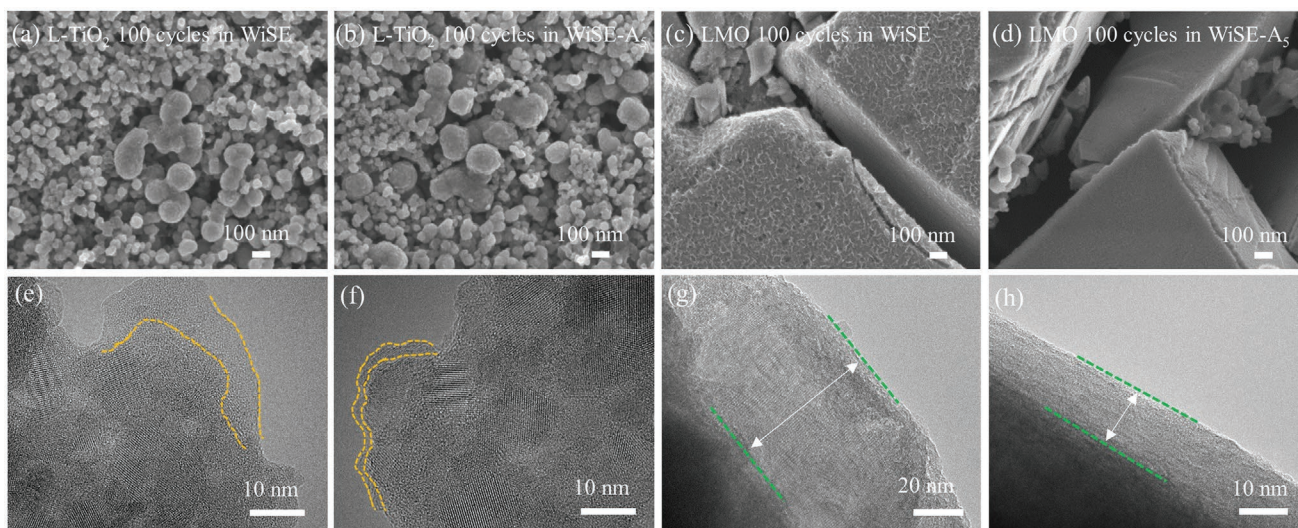
Conflict of Interest

The authors declare no conflict of interest.

Figure 6. SEM and HRTEM images of L-TiO$_2$ electrode after cycling in WiSE (a,e) and WiSE-A$_5$ (b,f) within 100 cycles, respectively; SEM and HRTEM images of LMO electrode after cycling in WiSE (c,g) and WiSE-A$_5$ (d,h) within 100 cycles, respectively.

Data Availability Statement

The data that support the findings of this study are available from the corresponding author upon reasonable request.

Keywords

[1] a) A. Eftekhari, *Adv. Energy Mater.* **2018**, *8*, 1801156; b) Z. Liu, Y. Huang, Y. Huang, Q. Yang, X. Li, Z. Huang, C. Zhi, *Chem. Soc. Rev.* **2020**, *49*, 180; c) W. Li, J. R. Dahn, D. S. Wainwright, *Science* **1994**, *264*, 1115.

[2] S. Lux, L. Terborg, O. Hachmöller, T. Placke, H. Meyer, S. Passerini, M. Winter, S. Nowak, *J. Electrochem. Soc.* **2013**, *160*, A1694.

[3] J. Luo, W. Cui, P. He, Y. Xia, *Nat. Chem.* **2010**, *2*, 760.

[4] L. Suo, O. Borodin, T. Gao, M. Olguin, J. Ho, X. Fan, C. Luo, C. Wang, K. Xu, *Science* **2015**, *350*, 938.

[5] Y. Yamada, K. Usui, K. Sodeyama, S. Ko, Y. Tateyama, A. Yamada, *Nat. Energy* **2016**, *1*, 16129.

[6] a) D. Liu, Q. Yu, S. Liu, K. Qian, S. Wang, W. Sun, X. Yang, F. Kang, B. Li, *J. Phys. Chem. C* **2019**, *123*, 12797; b) L. Suo, D. Oh, Y. Lin, Z. Zhuo, O. Borodin, T. Gao, F. Wang, A. Kushima, Z. Wang, H. Kim, *J. Am. Chem. Soc.* **2017**, *139*, 18670.

[7] C. Yan, R. Xu, Y. Xiao, J. Ding, L. Xu, B. Li, J. Huang, *Adv. Funct. Mater.* **2020**, *30*, 1909887.

[8] S. Ko, Y. Yamada, K. Miyazaki, T. Shimada, E. Watanabe, Y. Tateyama, T. Kamiya, T. Honda, J. Akikusa, A. Yamada, *Electrochem. Commun.* **2019**, *104*, 106488.

[9] L. Chen, J. Zhang, Q. Li, J. Vatamanu, X. Ji, T. Pollard, C. Cui, S. Hou, J. Chen, C. Yang, L. Ma, M. S. Ding, M. Garaga, S. Greenbaum, H. Lee, O. Borodin, K. Xu, C. Wang, *ACS Energy Lett.* **2020**, *5*, 968.

[10] L. Droguet, A. Grimaud, O. Fontaine, J. Tarascon, *Adv. Energy Mater.* **2020**, *10*, 2002440.

[11] F. Wang, Y. Lin, L. Suo, X. Fan, T. Gao, C. Yang, F. Han, Y. Qi, K. Xu, C. Wang, *Energy Environ. Sci.* **2016**, *9*, 3666.

[12] S. Kondou, E. Nozaki, S. Terada, M. L. Thomas, K. Ueno, Y. Umebayashi, K. Dokko, M. Watanabe, *J. Phys. Chem. C* **2018**, *122*, 20167.

[13] a) F. Wang, O. Borodin, M. S. Ding, M. Gobet, J. Vatamanu, X. Fan, T. Gao, N. Eidson, Y. Liang, W. Sun, S. Greenbaum, K. Xu, C. Wang, *Joule* **2018**, *2*, 927; b) J. Chen, J. Vatamanu, L. Xing, O. Borodin, H. Chen, X. Guan, X. Liu, K. Xu, W. Li, *Adv. Energy Mater.* **2019**, *10*, 1902654.

[14] a) D. Aurbach, K. Gamolsky, B. Markovsky, Y. Gofer, M. Schmidt, U. Heider, *Electrochim. Acta* **2002**, *47*, 1423; b) C. Korepp, H. Santner, T. Fujii, M. Ue, J. Besenhard, K. Möller, M. Winter, *J. Power Sources* **2006**, *158*, 578; c) K. Möller, H. Santner, W. Kern, S. Yamaguchi, J. Besenhard, M. Winter, *J. Power Sources* **2003**, *119*, 561.

[15] C. Korepp, W. Kern, E. Lanzer, P. Raimann, J. Besenhard, M. Yang, K. Möller, D. Shieh, M. Winter, *J. Power Sources* **2007**, *174*, 628.

[16] H. Santner, K. Möller, J. Ivančo, M. Ramsey, F. Netzer, S. Yamaguchi, J. Besenhard, M. Winter, *J. Power Sources* **2003**, *119*, 368.

[17] I. Stojković, N. Cvjetićanin, S. Mentus, *Electrochem. Commun.* **2010**, *12*, 371.

[18] a) L. Delle Site, C. F. Abrams, A. Alavi, K. Kremer, *Phys. Rev. Lett.* **2002**, *89*, 156103; b) C. Wang, C. Zou, Y. Cao, *J. Mol. Struct.* **2021**, *1228*, 129737.

[19] X. Hou, R. Wang, X. He, T. Pollard, X. Ju, L. Du, E. Paillard, H. Frielinghaus, L. Barnsley, O. Borodin, K. Xu, M. Winter, J. Li, *Angew. Chem., Int. Ed.* **2021**, *60*, 22812,

[20] L. Coustan, K. Zaghib, D. Bélanger, *J. Power Sources* **2018**, *399*, 299.

[21] J. Vatamanu, O. Borodin, *J. Phys. Chem. Lett.* **2017**, *8*, 4362.

[22] Y. Hu, H. Li, X. Huang, L. Chen, *Electrochem. Commun.* **2004**, *6*, 28.

[23] a) T. Hezard, K. Fajerwerg, D. Evrard, V. Collière, P. Behra, P. Gros, *J. Electroanal. Chem.* **2012**, *664*, 46; b) N. A. Zubair, N. A. Rahman, H. N. Lim, Y. Sulaiman, *Nanoscale Res. Lett.* **2017**, *12*, 113.

[24] X. Hou, X. Ju, W. Zhao, J. Wang, X. He, L. Du, B. Yan, J. Li, E. Paillard, J. Sun, *J. Power Sources* **2021**, *484*, 229255.

[25] K. Nie, X. Wang, J. Qiu, Y. Wang, Q. Yang, J. Xu, X. Yu, H. Li, X. Huang, L. Chen, *ACS Energy Lett.* **2020**, *5*, 826.